

Controlling the symmetry of the photonic spin Hall effect by an optical vortex pair

Weiming Zhen (甄蔚铭)¹, Xi-Lin Wang (汪喜林)¹, Jianping Ding (丁剑平)^{1,2,3,*} and Hui-Tian Wang (王慧田)¹

¹National Laboratory of Solid State Microstructures and School of Physics, Nanjing University, Nanjing 210093, People's Republic of China

²Collaborative Innovation Center of Advanced Microstructures, Nanjing University, Nanjing 210093, People's Republic of China

³Collaborative Innovation Center of Solid-State Lighting and Energy-Saving Electronics, Nanjing University, Nanjing 210093, People's Republic of China



(Received 23 February 2023; accepted 1 August 2023; published 18 August 2023)

A pair of vortices, one of the multiple vortices, exhibits more adjustable parameters and attractive characteristics compared with a single vortex. By introducing a vortex pair on the Gaussian beam, we not only realize both longitudinal and transverse asymmetrical spin splittings, but also achieve the symmetrical ones via the purely optical strategy. Namely, the symmetries of the spin splittings can be controlled flexibly by the tunable vortices, offering another degree of freedom for the photonic spin Hall effect. Based on the geometric phase theory, physical insights into the symmetry-controllable spin Hall shifts involving the initial phase from the incident vortex beam are provided. These findings reveal the influence of vortices on the symmetry of the photonic spin Hall effect and provide further potential methods for developing spin-based nanophotonic applications.

DOI: [10.1103/PhysRevA.108.023514](https://doi.org/10.1103/PhysRevA.108.023514)

I. INTRODUCTION

When a bounded beam is reflected from the interface, the spin-dependent splittings of left and right circularly polarized components occur in both longitudinal and transverse directions, called the photonic spin Hall effect (PSHE) [1–3]. It is a typical manifestation of the conservation of the spin angular momentum (SAM) and extrinsic orbital angular momentum (OAM) in the spin-orbit interaction of light and is regarded as an interesting optical analogy of the spin Hall effect in the electronic system. The PSHE is attributed to two types of well-known geometric phases: the spin-redirected Rytov-Vlasimirskii-Berry phase (RVB) and the Pancharatnam-Berry (PB) phase [4–6]. The former is related to the direction variations of the wave vector of the beam propagation; the latter is associated with the polarization state manipulation of the beam. Until now, many theoretical and experimental investigations have concentrated on enhancing the PSHE in different material interfaces such as glass [7], graphene [8,9], chiral materials [10], ENZ materials [11], liquid crystals [12], surface plasmon resonances (SPR) systems [13], inhomogeneous media [14], waveguide structures [15], quantum materials [16], Dirac materials [17], and anisotropic materials [18–20], as well as metamaterials [21,22]. Such studies are motivated by the numerous practical applications in various realms including identifying the layer of graphene [8], measuring the optical conductivity of graphene [9], optical spatial differentiation [23,24], and so on. In addition, the PSHE can also occur under the nonparaxial condition, especially in tight focusing [25,26].

Vortex beams [27,28], a kind of structured beams, carrying the intrinsic OAM and exhibiting the helical wavefront, as well as spatial phase singularity in the intensity distribution,

have been extensively studied because of their unique properties and applications such as optical trapping [29,30]. Laguerre-Gaussian beams (LGBs), as the earliest study of vortex beams, carrying the on-axis vortex and thus forming a “doughnut” shape, are solutions to the paraxial wave equation in cylindrical coordinates [31]. With the advances in technology, multiple vortices can be easily generated in laser by the spatial light modulator and the interactions between vortices and background fields have been studied [32–36]. Different from the single vortex, multiple vortices exhibit more fascinating characteristics. For example, a pair of vortices with the topological charge (TC) will mutually repel each other and rotate in opposite directions [35,36], while a pair of vortices with opposite TCs (known as the vortex dipole) will move toward, collide with, and even annihilate each other [32–34] in beams propagating in free space. It should be noted that little research has been carried out on the reflection from the incident beam with multiple vortices, let alone the vortex-vortex interactions through the reflection process.

In general, the PSHE manifests as the symmetrical spin-dependent splitting. However, there have been several interesting studies about asymmetric-dependent spin splitting. Zhou and Ling have reported the transverse asymmetric spin-dependent splitting under the elliptical polarization beam where the left and right circularly polarized components are unequal [37]. Under total internal reflection (TIR), the longitudinal asymmetric spin-dependent splitting has been achieved as well [38]. Due to the cross-coupling effect, the asymmetric PSHE can also be obtained in anisotropic materials [18]. On the other hand, the single vortex beam can generate the asymmetric PSHE owing to the intrinsic OAM involving the spin-orbit interactions [13,39–41], but they cannot generate symmetric spin splittings. The symmetry of the PSHE has not been flexibly controlled unless one is adjusting the materials parameters. We study here the PSHE involving multiple vortices, even though many

*jpding@nju.edu.cn

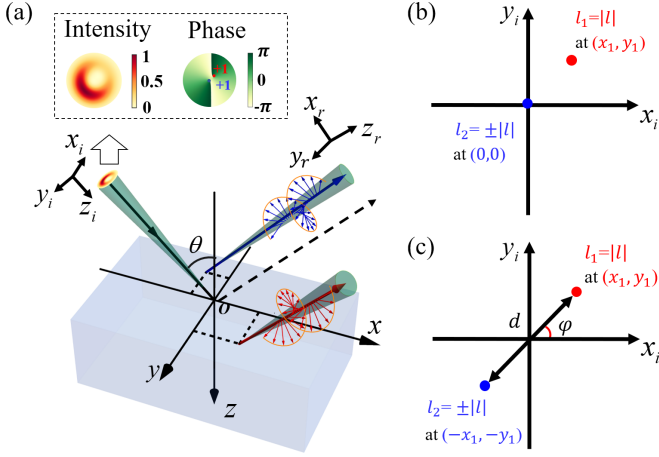


FIG. 1. (a) Schematic diagram of reflection for left ($\sigma = +1$) and right ($\sigma = -1$) circularly polarized components in the air-dielectric (glass) model. The solid and dashed black arrows represent the geometric paths of the incident and reflected beams, respectively. θ is the incident angle. Phase singularities of the vortex pair for (b) case 1, the second vortex is set as $(x_2, y_2) = (0, 0)$, and (c) case 2, the centrosymmetric vortex pair, $(x_2, y_2) = (-x_1, -y_1)$. The red and blue dots represent the first vortex core ($l_1 = |l|$) and the second one ($l_2 = \pm|l|$), respectively.

investigations about the PSHE with a single vortex have been reported. In view of such interesting characteristics of the multiple vortices, some natural questions arise. What about vortex-vortex interactions in the reflection process? What is the influence of the multiple vortices on the PSHE? More importantly, is there a simple method to flexibly manipulate the symmetry of the PSHE with the multiple vortices by the purely optical strategy or mechanism rather than restructuring the materials' structures?

In this contribution, we superpose a pair of vortices onto a Gaussian beam impinging on the air-dielectric (glass) interface to explore the PSHE. It is found that both transverse and longitudinal asymmetric spin splittings can be achieved. Different from the single on(off)-axis vortex reported in previous investigations [13,39–41], the positions (including the whole and relative positions) and the topological charge TC sign combination (i.e., the same TC sign and the opposite TC signs) of the vortex pair have also influenced the PSHE. Importantly, on the proper choice of the vortices' related positions and signs, both longitudinal and transverse symmetric spin splittings can also be obtained. Such intriguing findings are interpreted by the geometric phase theory, which is related

to the initial phase from the angular spectrum of the incident vortex beam, providing a flexible and simple treatment to directly control the symmetry of the PSHE in both longitudinal and transverse directions by our purely optical method.

II. THEORETICAL MODEL

The general reflection model to describe the PSHE is established as shown in Fig. 1, in which the laboratory coordinate system represented by (x, y, z) is attached to the air-dielectric (glass) interface at $z = 0$, while the local coordinate systems denoted by (x_i, y_i, z_i) and (x_r, y_r, z_r) are attached to the geometric paths of the incident and reflected beams, respectively. For the sake of simplicity, we will use superscript \parallel and \perp to mark the field vector parallel or orthogonal to the incident plane [i.e., the xOz plane in Fig. 1(a)]. The parallel (TM or p) polarization direction is located on the incident plane, i.e., along the x_i axial direction, while the orthogonal (TE or s) polarization direction is orthogonal to the incident plane, i.e., along the y_i axial direction. We consider a parallel polarized, paraxial, and monochromatic Gaussian beam carrying a pair of vortices with narrow continuous distributions of wave vector \mathbf{k} centered around $\mathbf{k}_0 = k_0 \hat{z}_i$ (where $k_0 = 2\pi/\lambda$ is a wave number with incident wavelength in vacuum and \hat{z}_i is a unit vector along the incident beam's central propagation direction). When the $kz - \omega t$ phase term is suppressed, the electric-field amplitude of such an incident beam can be written as follows:

$$\begin{aligned} E_i^{\parallel}(x_i, y_i) = \exp\left(-\frac{x_i^2 + y_i^2}{w_0^2}\right) \left(\frac{x_i - x_1}{w_0} + i\frac{y_i - y_1}{w_0}\right)^{|l|} \\ \times \left(\frac{x_i - x_2}{w_0} + i\operatorname{sgn}(l)\frac{y_i - y_2}{w_0}\right)^{|l|}, \end{aligned} \quad (1)$$

where w_0 is the beam waist and (x_1, y_1) and (x_2, y_2) are the positions of the two vortices with the same magnitude $|l|$ of the TCs. Here, the TC of the first vortex l_1 on (x_1, y_1) is always positive, i.e., $l_1 = |l|$, whereas the TC of the second one l_2 on (x_2, y_2) is $|l|$ or $-|l|$, depending on the sign of $|l|$ [as plotted in Figs. 1(b) and 1(c)]. Therefore, the same (opposite) TC of the vortex pair of the beam is also determined by the plus (minus) sign of l . Such sign combination forms the same vortices and the opposite vortices. For simplicity without loss of generality, we assume the low TC, $|l| = 1$, throughout this paper, except for the final discussion in the next section, which will expand to the high-order TC. The angular spectrum of the incident beam ($|l| = 1$) can be written as

(1) same vortices ($l_1 = 1, l_2 = 1$)

$$\tilde{E}_i^{\parallel}(k_{ix}, k_{iy}) = -\frac{1}{8} \exp\left[-\frac{1}{4}(k_{ix}^2 + k_{iy}^2)w_0^2\right] [(k_{ix} + ik_{iy})w_0^2 + 2(-ix_1 + y_1)][(k_{ix} + ik_{iy})w_0^2 + 2(-ix_2 + y_2)], \quad (2a)$$

(2) opposite vortices ($l_1 = 1, l_2 = -1$)

$$\begin{aligned} \tilde{E}_i^{\parallel}(k_{ix}, k_{iy}) = \frac{1}{8} \exp\left[-\frac{1}{4}(k_{ix}^2 + k_{iy}^2)w_0^2\right] \left\{ -w_0^4(k_{ix}^2 + k_{iy}^2) + 4(x_1 + iy_1)(x_2 - iy_2) \right. \\ \left. + 2w_0[2 + k_{ix}[i(x_1 + x_2 + iy_1) + y_2] + k_{iy}[x_1 - x_2 + i(y_1 + y_2)]] \right\}, \end{aligned} \quad (2b)$$

where Eqs. (2a) and (2b) show the cases of the same and opposite vortices, respectively, and k_{ix} as well as k_{iy} represent the longitudinal and transverse components of the incident wave vector \mathbf{k} individually. The angular spectrum of the reflected beam can be obtained considering the boundary conditions $k_{rx} = -k_{ix}$ and $k_{ry} = k_{iy}$ [42]:

$$\begin{pmatrix} \tilde{E}_r^{\parallel} \\ \tilde{E}_r^{\perp} \end{pmatrix} = \begin{pmatrix} r_p & \frac{k_{ry}(r_p+r_s)\cot\theta}{k_0} \\ -\frac{k_{ry}(r_p+r_s)\cot\theta}{k_0} & r_s \end{pmatrix} \begin{pmatrix} \tilde{E}_i^{\parallel} \\ \tilde{E}_i^{\perp} \end{pmatrix}. \quad (3)$$

Transforming the reflected electric fields in Eq. (2) from the linear polarization basis to the circular polarization basis by using the relation $\tilde{E}_r^{\pm} = [\tilde{E}_r^{\parallel} \mp i\tilde{E}_r^{\perp}]/\sqrt{2}$, we obtain

$$\begin{pmatrix} \tilde{E}_r^+ \\ \tilde{E}_r^- \end{pmatrix} = \frac{1}{\sqrt{2}} \begin{pmatrix} \frac{ir_p - r_s k_{ry} \cot\theta/k_0}{(i+k_{ry} \cot\theta/k_0)} & \frac{r_s + ir_p k_{ry} \cot\theta/k_0}{(i+k_{ry} \cot\theta/k_0)} \\ -\frac{r_s k_{ry} \cot\theta/k_0 + ir_p}{(k_{ry} \cot\theta/k_0 - i)} & \frac{r_s - ir_p k_{ry} \cot\theta/k_0}{(k_{ry} \cot\theta/k_0 - i)} \end{pmatrix} \begin{pmatrix} \tilde{E}_i^{\parallel} \\ \tilde{E}_i^{\perp} \end{pmatrix}, \quad (4)$$

where r_p and r_s are the Fresnel reflection coefficients of the polarization components parallel and orthogonal to the incidence plane in Fig. 1, respectively. By use of the Taylor series expansion of arbitrary spectral components around the central wave vector and considering only the first-order expansion term, the Fresnel reflection coefficients r_p and r_s can be expanded as

$$r_{p,s}(k_{ix}, k_{iy}) = r_{p,s}(k_{ix} = k_{iy} = 0) + k_{ix} \left[\frac{\partial r_{p,s}(k_{ix})}{\partial k_{ix}} \right]_{k_{ix}=k_{iy}=0} + k_{ix} \left[\frac{\partial r_{p,s}(k_{ix})}{\partial k_{iy}} \right]_{k_{ix}=k_{iy}=0}, \quad (5)$$

where $\frac{\partial r_{p,s}(k_{ix})}{\partial k_{ix}}|_{k_{ix}=k_{iy}=0} = \frac{\partial r_{p,s}(\theta)}{\partial \theta}$ and $\frac{\partial r_{p,s}(k_{ix})}{\partial k_{iy}}|_{k_{ix}=k_{iy}=0} = 0$. In the air-dielectric (glass) structure, we have

$$r_p(\theta) = \frac{\varepsilon \cos\theta - \sqrt{\varepsilon - \sin^2\theta}}{\varepsilon \cos\theta + \sqrt{\varepsilon - \sin^2\theta}}, \quad r_s(\theta) = \frac{\cos\theta - \sqrt{\varepsilon - \sin^2\theta}}{\cos\theta + \sqrt{\varepsilon - \sin^2\theta}}. \quad (6)$$

Therefore, the longitudinal (in x_r direction) and transverse (in y_r direction) spin shifts ($z_r = 0$) for the left ($\sigma = +1$) and right ($\sigma = -1$) circularly polarized components of the reflected field can be calculated by

$$\delta_\sigma^x = \frac{\iint x_r |E_r^\sigma(x_r, y_r)|^2 dx_r dy_r}{\iint |E_r^\sigma(x_r, y_r)|^2 dx_r dy_r} - \frac{\iint x_i |E_i^\sigma(x_i, y_i)|^2 dx_i dy_i}{\iint |E_i^\sigma(x_i, y_i)|^2 dx_i dy_i}, \quad (7)$$

$$\delta_\sigma^y = \frac{\iint y_r |E_r^\sigma(x_r, y_r)|^2 dx_r dy_r}{\iint |E_r^\sigma(x_r, y_r)|^2 dx_r dy_r} - \frac{\iint y_i |E_i^\sigma(x_i, y_i)|^2 dx_i dy_i}{\iint |E_i^\sigma(x_i, y_i)|^2 dx_i dy_i}. \quad (8)$$

Owing to the effect of the OAM of a pair of vortices, it is possible to flexibly regulate the symmetry of the longitudinal

and transverse PSHEs, which can be well demonstrated by the following cases in the next section.

III. MANIPULATING SYMMETRY OF SPIN SPLITTINGS VIA OPTICAL VORTICES

Here we choose the incident wavelength $\lambda = 532$ nm, the beam waist $w_0 = 20$ μm , and the relative dielectric constant of the glass $\varepsilon = 1.515^2$ in the numerical simulation.

A. Case 1: The position of the second vortex is $(x_2, y_2) = (0, 0)$

In the first case, the position of the second vortex is fixed at the coordinate origin, i.e., $x_2 = y_2 = 0$, as shown in Fig. 1(b). The expressions of the longitudinal and transverse spin shifts for the Gaussian vortex beam ($|l| = 1$, i.e., $l_1 = 1, l_2 = \pm 1$) can be calculated by using Eqs. (7) and (8) as

(1) same vortices ($l_1 = 1, l_2 = 1$)

$$\delta_\sigma^x = \frac{w_0^4 x_1 (A_1 + \sigma B_1)}{2(C_1 + D_1)} + \frac{w_0^2 x_1}{w_0^2 + x_1^2 + y_1^2}, \quad (9a)$$

$$\delta_\sigma^y = \frac{-w_0^4 (E_1 + \sigma F_1 + G_1)}{2(C_1 + D_1)} + \frac{w_0^2 y_1}{w_0^2 + x_1^2 + y_1^2}, \quad (9b)$$

where $A_1 = 2k^2 w_0^2 r_p^2 + 3\chi^2$, $B_1 = \cot\theta(r_p + r_s)[5\cot\theta(r_p + r_s) + 4\chi]$, $C_1 = k^2 w_0^4 r_p^2 (w_0^2 + x_1^2 + y_1^2) + 4k\chi w_0^4 y_1 r_p$, $D_1 = (\cot^2\theta + \chi^2)(r_p + r_s)^2 [2w_0^2(x_1^2 + y_1^2) + 3w_0^4]$, $E_1 = 2k^2 w_0^2 y_1 r_p^2 + 2k\chi r_p (2w_0^2 + x_1^2 + y_1^2)$, $F_1 = 2\cot\theta(r_p + r_s)[kr_p(w_0^2 + x_1^2 + y_1^2) + 2\chi y_1]$, and $G_1 = 3y_1 \cot^2\theta(r_p + r_s)^2 + 5\chi^2 y_1$, in which $\chi = \frac{\partial r_p(\theta)}{\partial \theta}$, $r_p = r_p(\theta)$, and $r_s = r_s(\theta)$, and (2) opposite vortices ($l_1 = 1, l_2 = -1$)

$$\delta_\sigma^x = \frac{w_0^4 x_1 [2k^2 w_0^2 r_p^2 + \cot^2\theta(r_p + r_s)^2 + 3\chi^2]}{2(A'_1 + B'_1)} + \frac{w_0^2 x_1}{w_0^2 + x_1^2 + y_1^2}, \quad (10a)$$

$$\delta_\sigma^y = \frac{w_0^4 (C'_1 + \sigma D'_1 + E'_1)}{2(A'_1 + B'_1)} + \frac{w_0^2 y_1}{w_0^2 + x_1^2 + y_1^2}, \quad (10b)$$

where $A'_1 = k^2 w_0^4 r_p^2 (w_0^2 + x_1^2 + y_1^2)$, $B'_1 = [\cot^2\theta(r_p + r_s)^2 \chi^2 + 2w_0^2(x_1^2 + y_1^2) + w_0^4]$, $C'_1 = 2k^2 w_0^2 y_1 r_p^2$, $D'_1 = 2k\cot\theta r_p(r_p + r_s)(w_0^2 + x_1^2 + y_1^2)$, and $E'_1 = 2k\chi r_p(x_1^2 + y_1^2) + 3y_1 \cot^2\theta(r_p + r_s)^2 + \chi^2 y_1$.

Let us analyze the first situation with the same vortices. Figures 2(a) and 2(b) show the asymmetry distribution of δ_σ^x and δ_σ^y with the incident angle θ . It can also be seen from Eqs. (9a) and (9b) that there are both longitudinal and transverse asymmetric PSHEs all the time due to the existence of σB_1 and σF_1 induced by the OAM of the vortex pair. It should be noted that, when the polarization state is parallel polarized, the longitudinal spin splitting disappears usually in the isotropic medium except by changing the polarization states [38] or utilizing the anisotropic medium [18]. Without changing the state of polarization (i.e., keeping the parallel polarization), imposing vortices on the Gaussian profile can also achieve asymmetric PSHEs, which is another method to obtain the nonzero longitudinal PSHE in the general medium. Different from the single vortex, the TC sign combination of

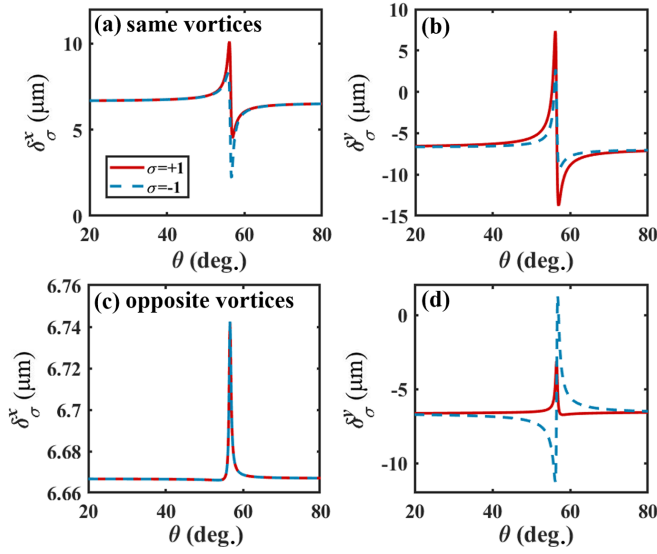


FIG. 2. (a), (c) Variations of longitudinal spin shifts δ_σ^x as well as (b) and (d) transverse spin shifts δ_σ^y with respect to the incident angle θ . The solid and dashed curves represent the left and right circularly polarized components, respectively. The TC of the second vortex is positive ($l_2 = 1$, the first row) and negative ($l_2 = -1$, the second row). Here, the position of the first vortex is chosen as $x_1 = 10 \mu\text{m}$ and $y_1 = 10 \mu\text{m}$ and the position of the second vortex is fixed at the coordinate origin.

vortices has an impact on the spin splittings. In another situation, the transverse spin shifts δ_σ^y with the opposite vortices of the oppositely circularly polarized components are also asymmetric [as shown in Figs. 2(c) and 2(d)] owing to the existence in Eq. (10b), while the longitudinal shifts δ_σ^x of oppositely circularly polarized components overlap because the

longitudinal shifts are spin-independent in this situation as indicated by Eq. (10a). Therefore, the sign combination of the TCs of the vortices is another key factor in regulating PSHEs. This is why we focus on the TC sign combination (including the same sign and the opposite signs) in the vortex pair, enabling more degree of freedom than the single vortex. The relative positions of the two vortices also have an influence on the PSHEs. Due to the fixed position of the second vortex, we explore the effect of the position of the first vortex on the PSHEs. The spin shift and the shift difference, $\Delta^{x,y} = \delta_{+1}^{x,y} - \delta_{-1}^{x,y}$, between oppositely circularly polarized components with the same vortices are plotted in Fig. 3 versus (x_1, y_1) . It is easy to find that both longitudinal and transverse spin shifts show a strong dependence on the positions of x_1 and y_1 . It means that the magnitudes and directions of PSHEs can be tuned easily by adjusting the positions of the vortices. Comparison between Figs. 3(a) and 3(b), as well as between Figs. 3(d) and 3(e), shows the same trend (but different values) on x_1 and y_1 for left and right circularly polarized components. Interestingly, $\Delta^{x,y}$ also have a similar tendency on x_1 and y_1 . On the other hand, the PSHEs with the opposite vortices are also dependent on the positions of x_1 and y_1 , as illustrated in Fig. 4. However, different from Fig. 3, due to the effect of different signs of the TCs, the corresponding results of the situation with the opposite vortices changed, as shown in Fig. 4. It should be noted that there is a whole and nonsplitting longitudinal shift as seen from Eq. (10a), so Δ^x is always zero [as shown in Fig. 4(c)].

To clarify the basic physical picture of the asymmetric PSHE induced by the vortex pair, the numerical results of the intensity and phase distribution of the initial fields and the Stokes parameter S_3 of the reflected fields are discussed for different vortices' positions as shown in Fig. 5 with the same TC. Due to the effect of the vortices, the incident intensity

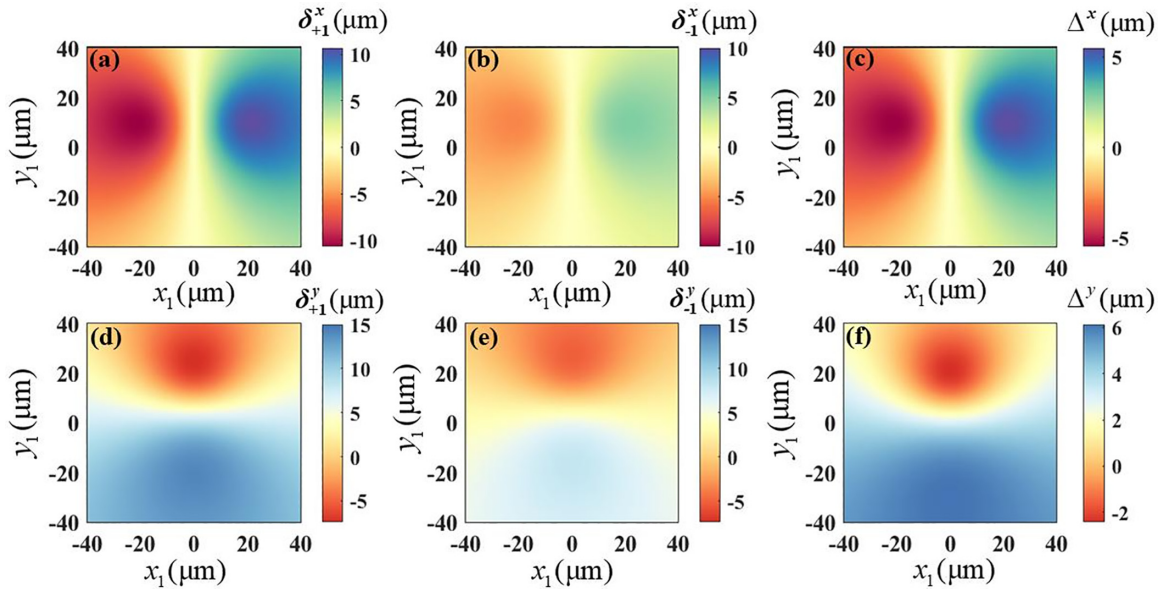


FIG. 3. (a), (b) Longitudinal spin shifts δ_σ^x and (d) and (e) transverse spin shifts δ_σ^y of left ($\sigma = +1$) and right ($\sigma = -1$) circularly polarized components versus the position of the first vortex. (c), (f) The spin shift variations difference $\Delta^{x,y} = \delta_{+1}^{x,y} - \delta_{-1}^{x,y}$ between oppositely circularly polarized components. The incident angle is chosen as $\theta = 56.4^\circ$ (near the Brewster angle $\theta_B = 56.57^\circ$); the second vortex is fixed at the coordinate origin and its TC is positive ($l_2 = 1$).

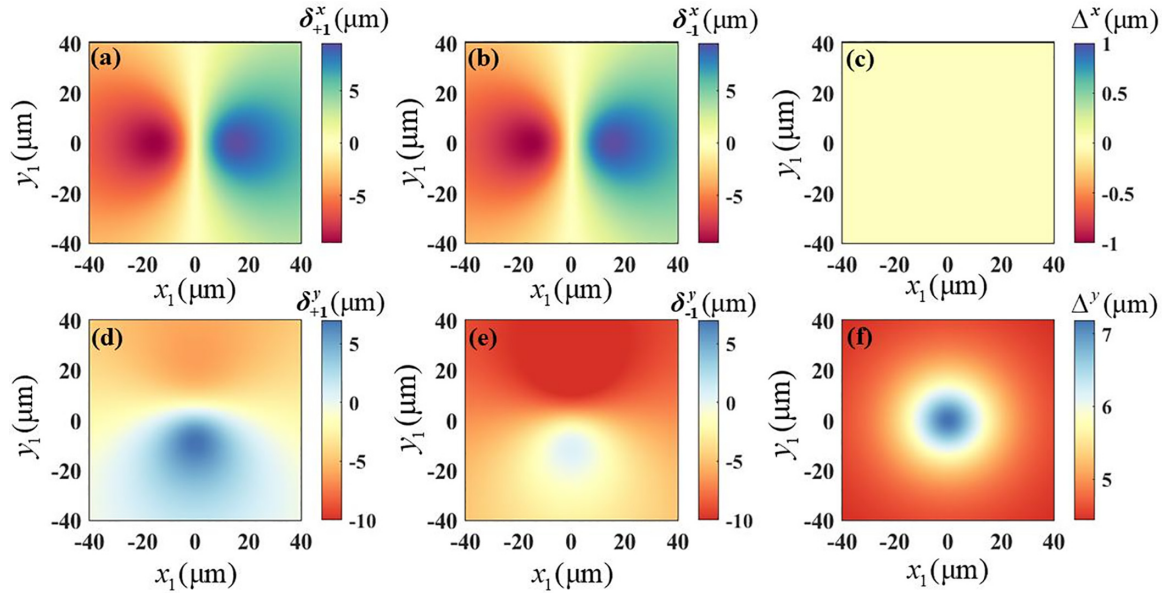


FIG. 4. (a), (b) Longitudinal spin shifts δ_{σ}^x and (d) and (e) transverse spin shifts δ_{σ}^y of left ($\sigma = +1$) and right ($\sigma = -1$) circularly polarized components versus the position of the first vortex. (c), (f) The spin shift variations difference $\Delta^{x,y} = \delta_{+1}^{x,y} - \delta_{-1}^{x,y}$ between oppositely circularly polarized components. The incident angle is chosen as $\theta = 56.4^\circ$ (near the Brewster angle $\theta_B = 56.57^\circ$); the second vortex is fixed at the coordinate origin and its TC is negative ($l_2 = -1$).

distribution breaks the circular symmetry of the Gaussian profile and hence after reflection the situation becomes more complicated. There are asymmetrical intensity distributions of opposite spin states, where the left circularly polarized component ($S_3 > 0$) is less than the right polarized component ($S_3 < 0$), resulting in the asymmetrical PSHEs. More interestingly, when the first vortex is far away from the center of the Gaussian profile [$x_1 = y_1 = 30 \mu\text{m}$, as illustrated in Fig. 5(d)], the incident intensity distribution is still affected by this vortex

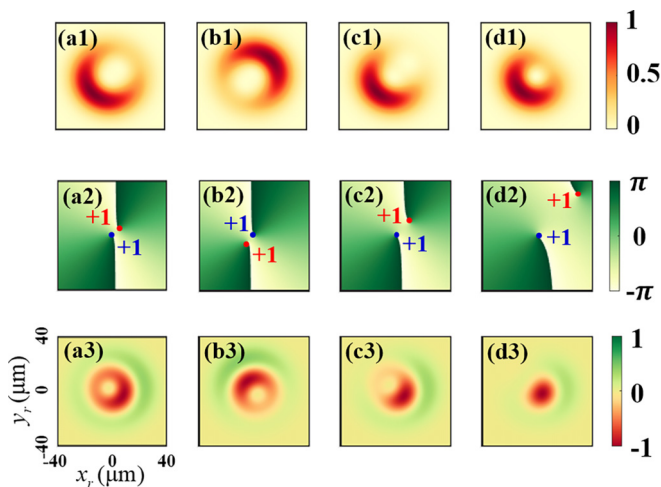


FIG. 5. Transverse intensity (the first row) and phase distribution (the second row) of the incident beam, and Stokes parameter S_3 of the reflected beam (the third row) for different positions of the first vortex: (a) $x_1 = y_1 = 5 \mu\text{m}$, (b) $x_1 = y_1 = -5 \mu\text{m}$, (c) $x_1 = y_1 = 10 \mu\text{m}$, and (d) $x_1 = y_1 = 30 \mu\text{m}$. The incident angle is $\theta = 56.4^\circ$ (near the Brewster angle $\theta_B = 56.57^\circ$); the second vortex is fixed at the coordinate origin and its TC is positive ($l_2 = 1$).

and thus both longitudinal and transverse asymmetric PSHEs are also obtained. Therefore, the off-axis vortex (even far from the center of the Gaussian profile) plays an important role in producing the asymmetric PSHEs. Similarly, the corresponding intensity and phase distribution of the incident beam and S_3 of the reflected beam with the opposite vortices are also plotted in Fig. 6. Despite carrying the opposite TCs, the intensity distributions of the incident beams are the same as those with the same TC by comparing Figs. 5(a1)–5(d1) and Figs. 6(a1)–6(d1). However, thanks to the fact that the effect of the opposite vortices is distinct from that of the same

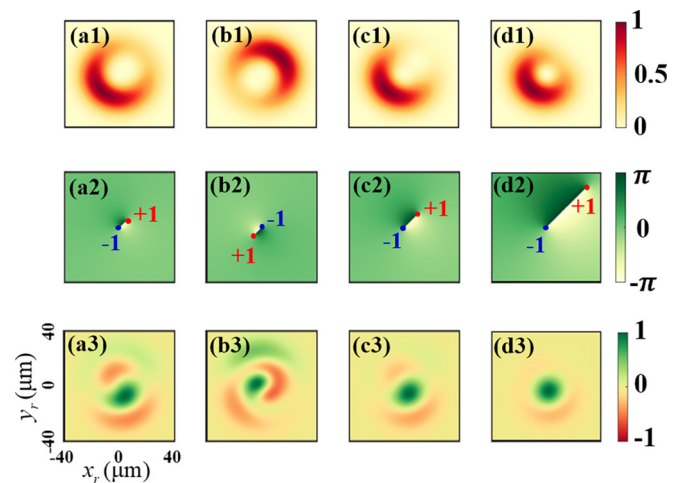


FIG. 6. Transverse intensity (the first row) and phase distribution (the second row) of the incident beam, and Stokes parameter S_3 of the reflected beam (the third row). Here, the second vortex is fixed at the coordinate origin and its TC is negative ($l_2 = -1$). Other parameters are the same as those in Fig. 5.

vortices, the different behaviors of the Stokes parameter S_3 of the reflected beam occur, resulting in different longitudinal and transverse PSHEs.

B. Case 2: The positions of the two vortices are centrosymmetric, $(x_2, y_2) = (-x_1, -y_1)$

In the second case, differently, we change the positions of the two vortices, which are centrosymmetric, i.e., $x_2 = -x_1$, $y_2 = -y_1$, as shown in Fig. 1(c). The expressions of the spin shifts of Eqs. (9) and (10) can be changed as

(1) same vortices ($l_1 = 1, l_2 = 1$)

$$\delta_\sigma^x = \frac{4kr_p w_0^4 \chi x_1 y_1}{A_2 + B_2 + C_2}, \quad (11a)$$

$$\delta_\sigma^y = \frac{-(D_2 + \sigma E_2)}{A_2 + B_2 + C_2}, \quad (11b)$$

where $A_2 = \cot^2 \theta (r_p + r_s)^2 [3w_0^4 + 2w_0^2 (y_1^2 - x_1^2) + 2(x_1^2 + y_1^2)^2]$, $B_2 = k^2 r_p^2 w_0^2 [w_0^4 + 2(x_1^2 + y_1^2)^2]$, $C_2 = \chi^2 [3w_0^4 + 2w_0^2 (x_1^2 - y_1^2) + 2(x_1^2 + y_1^2)^2]$, $D_2 = 2w_0^2 \chi (w_0^2 + x_1^2 - y_1^2)$, and $E_2 = \cot \theta (r_p + r_s) [w_0^4 + 2(x_1^2 + y_1^2)^2]$, and

$$\delta_\sigma^x = \frac{4\sigma \chi w_0^2 x_1 \cot \theta (r_p + r_s) (x_1^2 + y_1^2)}{A'_2 + B'_2 + C'_2 + D'_2}, \quad (12a)$$

$$\delta_\sigma^y = \frac{-\sigma w_0^2 \cot \theta (r_p + r_s) \{kr_p [w_0^4 + 2(x_1^2 + y_1^2)^2] + 4\chi y_1 (x_1^2 + y_1^2)\}}{A'_2 + B'_2 + C'_2 + D'_2}, \quad (12b)$$

where $A'_2 = k^2 w_0^2 r_p^2 [w_0^4 + 2(x_1^2 + y_1^2)^2]$, $B'_2 = 8k w_0^2 \chi y_1 r_p (x_1^2 + y_1^2)$, $C'_2 = \cot^2 \theta (r_p + r_s)^2 [2w_0^2 (3x_1^2 + y_1^2) + w_0^4 + 2(x_1^2 + y_1^2)^2]$, and $D'_2 = \chi^2 [2w_0^2 (x_1^2 + 3y_1^2) + w_0^4 + 2(x_1^2 + y_1^2)^2]$. In this case, in order to further explore the influence of the relative and whole positions of vortices on the PSHE, we introduce the relative distance $d = \sqrt{(x_1 - x_2)^2 + (y_1 - y_2)^2}$ between the two vortices and the vortices' whole azimuth angle $\varphi = \arctan(\frac{y_1 - y_2}{x_1 - x_2})$, as shown in Fig. 1(c). The dependences of the longitudinal and transverse spin shifts on the relative distance d and the whole azimuth angle φ are shown by the polar coordinates (d, φ) in Fig. 7 (the same vortices) and Fig. 8 (the opposite vortices). In this situation with the same vortices, one can observe from Eq. (11) that the longitudinal spin shifts δ_σ^x are overlapped, while the transverse spin shifts δ_σ^y of oppositely circularly polarized components are asymmetric, which are consistent with the representation of Fig. 7. It also can be seen that from Fig. 7, when the whole azimuth angle φ rotates 180° counterclockwise, δ_σ^x and δ_σ^y are the same values where there are the same settings of the positive vortex pair. Meanwhile, the transverse spin shifts are also symmetric along the x axis and y axis, respectively, because δ_σ^y is an even function of x_1 and y_1 as represented by Eq. (11b). When the relative distance d remains the same, for various vortices' whole azimuth angles φ , however, different longitudinal and transverse spin shifts occur and vice versa. Consequently, the magnitude and direction of δ_σ^x and δ_σ^y can be manipulated by changing the vortices' relative positions as well as their whole positions. Significantly,

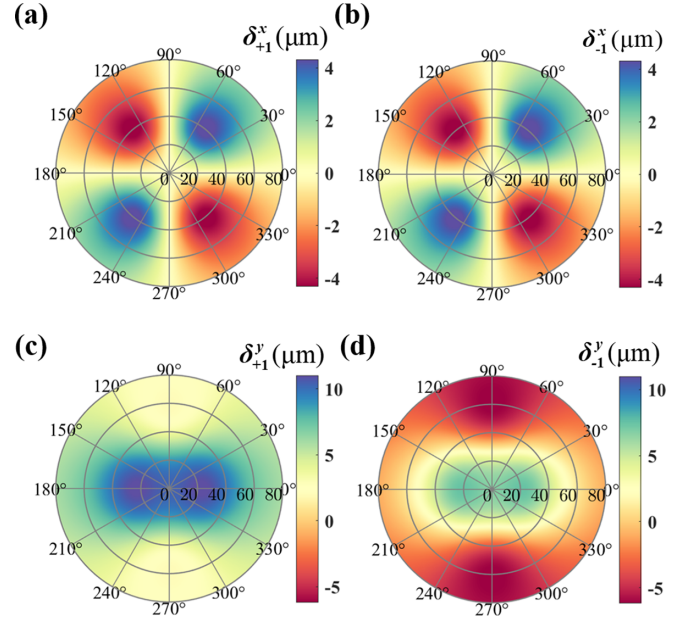


FIG. 7. (a), (b) δ_σ^x and (c), (d) δ_σ^y of left ($\sigma = +1$) and right ($\sigma = -1$) circularly polarized components versus the relative position between the same vortices: (radial) the relative distance d and (angular) the whole azimuth angle φ of vortices. The incident angle is $\theta = 56.4^\circ$ (near the Brewster angle $\theta_B = 56.57^\circ$).

in the situation with opposite vortices, both longitudinal and transverse spin shifts return to being symmetric as indicated by Eq. (12), which can also be clearly observed in Fig. 8. Hence, in addition to achieving both longitudinal and transverse asymmetric PSHEs via the above-mentioned

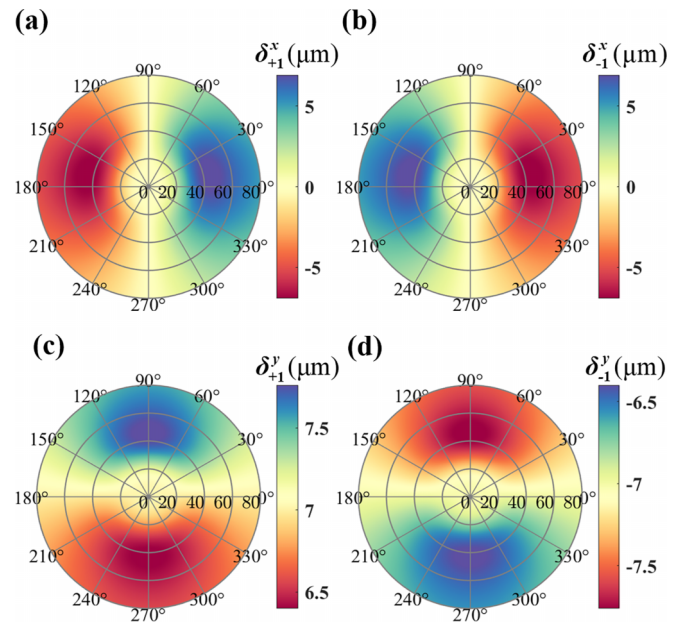


FIG. 8. (a), (b) δ_σ^x and (c), (d) δ_σ^y of left ($\sigma = +1$) and right ($\sigma = -1$) circularly polarized components versus the relative position between the opposite vortices: (radial) the relative distance d and (angular) the whole azimuth angle φ of vortices. Other parameters are the same as those in Fig. 7.

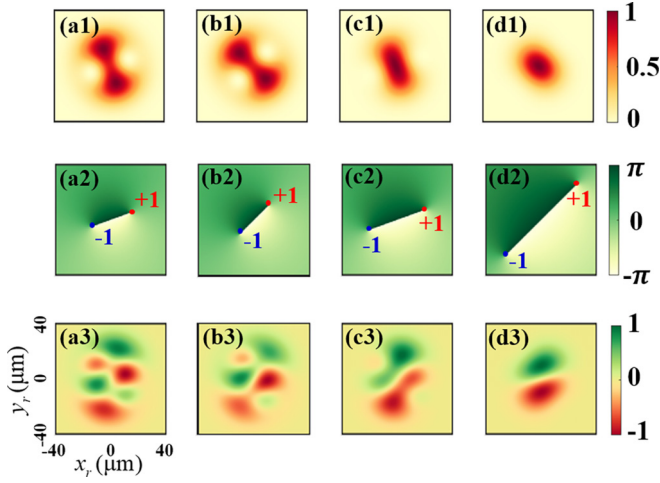


FIG. 9. Transverse intensity (the first row) and phase distribution (the second row) of the incident beam, and Stokes parameter S_3 of the reflected beam (the third row). Here, the two vortices are centrosymmetric and the TC of the second one is negative ($l_2 = -1$): for different related positions of vortices (a) $d = 30 \mu\text{m}$, $\varphi = 20^\circ$, (b) $d = 30 \mu\text{m}$, $\varphi = 45^\circ$, (c) $d = 45 \mu\text{m}$, $\varphi = 20^\circ$, and (d) $d = 75 \mu\text{m}$, $\varphi = 45^\circ$. Other parameters are the same as those in Fig. 5.

vortex configurations, the symmetric PSHEs can also be obtained if the positions of the two vortices with opposite TCs are centrosymmetric. That is to say, the symmetry of the PSHE can also be flexibly and effectively regulated and controlled by these vortices' positions (including the whole and relative positions) and their TC sign combination. Therefore, this is a significant result in this paper. Note that the single on(off)-axis vortex beam is unable to achieve the symmetric PSHE, which will be elaborated upon later. In addition, the corresponding S_3 is also plotted in Fig. 9. Different from Figs. 5 and 6, the reflected field distributions of the left ($S_3 > 0$) and right ($S_3 < 0$) circularly polarized components exhibit the symmetric structures, leading to both longitudinal and transverse symmetric spin shifts (as shown in Fig. 9). Therefore, the positions and signs of vortices determine the symmetry properties of the opposite spin components of the reflected beam. This leads to the fact that different vortices may demonstrate some different symmetry properties in the PSHEs in the reflected beam.

C. Physical insights of the symmetry of the PSHE

Due to the similarities in the physics of transverse and longitudinal spin displacements, we exclusively employ transverse examples here for the purpose of illustration. As reported in previous articles [13,39–41], the expressions of the PSHE of the vortex beam become more complicated, involving the intrinsic OAM in the spin-orbit interactions. In fact, the single vortex beam can only induce the asymmetrical PSHE, which can be explained by the view of the geometric phase (see the Appendix for details). To satisfy the transversality of photon polarization through the reflection process, the polarization rotation in momentum space occurs and generates a geometric phase gradient, thus inducing the PSHE. For the parallelly polarized incident beam, the ob-

tained geometric phase of the reflected beam of opposite spin states can be represented as $\Phi_{G,p}(\sigma) = -\sigma \frac{r_p + r_s}{r_p} \frac{k_{ry}}{k} \cot \theta$, and the corresponding transverse spin shifts depend on the gradient of the total phase $\delta_\sigma^y = -\nabla_{k_{ry}} \Phi_{Tot,p}(\sigma) = \nabla_{k_{ry}} \Phi_{G,p}(\sigma) = -\sigma \frac{\cot \theta}{k_0} (1 + \frac{r_s}{r_p})$, where $\Phi_{Tot,p}(\sigma)$ is the total phase for each spin component of the reflected beam (see the Appendix for details). The effect of a single vortex manifests as an initial momentum-dependent phase $\Phi_{int,p}(k_{ix}, k_{iy})$ in the incident beam. This phase $\Phi_{int,p}(k_{ix}, k_{iy})$ interacts with the geometric phase $\Phi_{G,p}(\sigma)$, resulting in the formation of a total phase $\Phi_{Tot,p}(\sigma)$ that originally consisted solely of the geometric phase $\Phi_{G,p}(\sigma)$. Consequently, asymmetrical spin splittings occur instead of symmetrical ones. It is clear that the initial momentum-dependent phase $\Phi_{int,p}(k_{ix}, k_{iy})$ is the physical origin of the asymmetrical spin shifts and thus breaks the symmetry of the PSHE. It should be mentioned that the interesting and significant result in this work is that, compared with the single vortex beam, the symmetrical PSHE can be obtained even under the effect of the two vortices, owing to the fact that the angular spectrums of our incident beam with vortex pair can possess the momentum-dependent initial phase (like the single vortex) and can also be not equipped with it, depending on their positions and TC sign combination. Take the second case (the positions of the vortices are centrosymmetric), for example: in the same TC situation, Eq. (2a) becomes

$$\tilde{E}_i^{\parallel}(k_{ix}, k_{iy}) = -\frac{1}{8} e^{-\frac{1}{4}(k_{ix}^2 + k_{iy}^2)w_0^2} \times [(k_{ix} + ik_{iy})^2 w_0^4 + 4(x_1 + iy_1)^2]. \quad (13)$$

It can be seen that the incident angular spectrum involves the vortex-induced momentum-dependent initial phase $\Phi_{int,p}(k_{ix}, k_{iy})$ and thus generates the asymmetrical PSHE, while in the opposite TC situation, Eq. (2b) can be changed as

$$\tilde{E}_i^{\parallel}(k_{ix}, k_{iy}) = -\frac{1}{8} e^{-\frac{1}{4}(k_{ix}^2 + k_{iy}^2)w_0^2} [(k_{ix}^2 + k_{iy}^2)w_0^4 - 4w_0^2(1 + k_{iy}x_1 - k_{ix}y_1) + 4(x_1^2 + y_1^2)], \quad (14)$$

where there is no initial phase, let alone the initial momentum-dependent phase. In this situation, therefore, the PSHE returns to the symmetrical spin splittings. Namely, the vortex pair has the function of adjusting the symmetry of the PSHE, compared with the single vortex. In terms of the effect on the symmetry, interestingly, the two vortices with opposite TCs “cancel” each other, like annihilating each other in beam propagation due to the vortex-vortex interactions [32–34]. On the other hand, anisotropic material structures can also incorporate the geometric phase to yield symmetrical or asymmetrical spin splittings based on the cross-coupling effect. However, their fabrication processes are very complex and thus costly, compared with isotropic material structures. Therefore, our scheme using the incident beam with the vortex pair enables controlling the symmetry of the PSHE more flexibly and economically, by using purely optical treatment rather than restructuring the materials structures, and provides different physical insights into the symmetry of the PSHE.

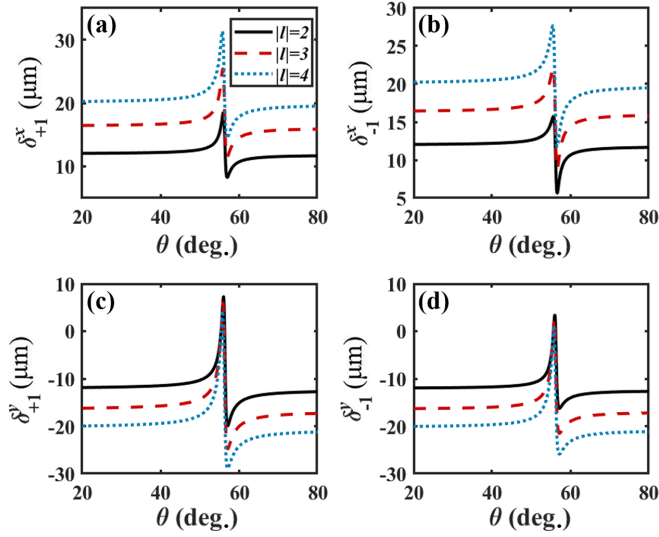


FIG. 10. Variations of longitudinal spin shifts δ_{σ}^x (the first row) and transverse spin shifts δ_{σ}^y (the second row) of left (the left column) and right (the right column) circularly polarized components with respect to the incident angle for different orders of TCs: $|l| = 2$ (solid line), $|l| = 3$ (dashed line), and $|l| = 4$ (dotted line). The TC of the second vortex is positive ($l_2 = |l|$). Other parameters are the same as those in Fig. 2.

D. Case of the high-order TC

Last but not least, we generalize our discussion to the case of the high-order TCs of vortices. Here, by directly using numerical integrations of Eqs. (7) and (8), the corresponding results are illustrated in Fig. 10. It is easy to find that, with the increasing $|l|$, the longitudinal and transverse spin shifts increase as well, which is similar to that of the LGB with the single. It is easy to find that, with the increasing $|l|$, the longitudinal and transverse spin shifts increase as well, which is similar to that of the LGB with the single vortex [13]. Therefore, the giant and symmetry-controllable PSHEs are desirable in this work.

IV. CONCLUSION

As a summary, we theoretically demonstrate the longitudinal and transverse symmetry-tunable PSHEs generated by the Gaussian beam carrying a pair of vortices. Besides the magnitudes and directions of these spin shifts, their symmetries can be regulated by adjusting the vortices' positions (including the whole and relative positions) as well as their TC sign combination (exhibiting the same vortices and the opposite vortices). Such important findings are physically explained from the perspective of the geometric phase, offering a different and effective purely optical strategy for flexibly controlling the symmetry of the PSHE in both longitudinal and transverse directions via appropriate settings of the vortices. In addition, these findings can be applied to the case of high-order TCs. Our investigations reported here deepen the understanding of the PSHE induced by the vortices, facilitate further research on the vortex-vortex interactions in the reflection process, and open up the prospect for potential applications in adjustable spin-based photoelectric devices.

ACKNOWLEDGMENTS

This research is supported in part by the National Key R&D Program of China (Grants No. 2022YFA1404800 and No. 2018YFA0306200), by the National Science Foundation of China (Grants No. 12234009 and No. 12274215), and by the Postgraduate Research & Practice Innovation Program of Jiangsu Province (Grant No. KYCX23_0099).

APPENDIX: RELATION BETWEEN GEOMETRIC PHASES AND PHOTONICS SPIN HALL SHIFTS

The relation between the incident and the reflected angular spectrums, represented by the linear polarization basis and the circular polarization basis, respectively, from Eq. (4) in the main text is

$$\begin{pmatrix} \tilde{E}_r^+ \\ \tilde{E}_r^- \end{pmatrix} = \frac{1}{\sqrt{2}} \begin{pmatrix} \frac{ir_p - r_s k_{ry} \cot \theta / k_0}{(i + k_{ry} \cot \theta / k_0)} & \frac{r_s + ir_p k_{ry} \cot \theta / k_0}{(i + k_{ry} \cot \theta / k_0)} \\ -\frac{r_s k_{ry} \cot \theta / k_0 + ir_p}{(k_{ry} \cot \theta / k_0 - i)} & \frac{r_s - ir_p k_{ry} \cot \theta / k_0}{(k_{ry} \cot \theta / k_0 - i)} \end{pmatrix} \begin{pmatrix} \tilde{E}_i^{\parallel} \\ \tilde{E}_i^{\perp} \end{pmatrix}. \quad (\text{A1})$$

By introducing this approximation $1 + i\left(\frac{r_p + r_s}{r_{p/s}} \frac{k_{ry}}{k} \cot \theta\right) \approx \exp\left(i\frac{r_p + r_s}{r_{p/s}} \frac{k_{ry}}{k} \cot \theta\right)$, the expression in Eq. (A1) can be transformed as follows:

$$\begin{pmatrix} \tilde{E}_r^+ \\ \tilde{E}_r^- \end{pmatrix} = \frac{1}{\sqrt{2}} \begin{pmatrix} \frac{\exp\left[i\left(\frac{r_p + r_s}{r_p} \frac{k_{ry}}{k} \cot \theta\right)\right]}{r_p} & \frac{-i \exp\left[i\left(\frac{r_p + r_s}{r_s} \frac{k_{ry}}{k} \cot \theta\right)\right]}{r_s} \\ \frac{\exp\left[-i\left(\frac{r_p + r_s}{r_p} \frac{k_{ry}}{k} \cot \theta\right)\right]}{r_p} & \frac{i \exp\left[-i\left(\frac{r_p + r_s}{r_s} \frac{k_{ry}}{k} \cot \theta\right)\right]}{r_s} \end{pmatrix} \begin{pmatrix} \tilde{E}_i^{\parallel} \\ \tilde{E}_i^{\perp} \end{pmatrix}, \quad (\text{A2})$$

where $\Phi_{Tot,p}(\sigma)$ is the total phase for each spin component of the reflected beam and $\Phi_{G,p}(\sigma) = -\Phi_{Tot,p}(\sigma) = -\sigma \frac{r_p + r_s}{r_p} \frac{k_{ry}}{k} \cot \theta$, $\Phi_{G,s}(\sigma) = -\Phi_{Tot,p}(\sigma) = -\sigma \frac{r_p + r_s}{r_s} \frac{k_{ry}}{k} \cot \theta$ are the corresponding geometric phases through the reflected process from the incident parallel and orthogonal polariza-

tion beams, respectively, including the RVB phase and the PB phase, for every spin component of the reflected beam consisting of the spin-maintained normal mode exhibiting the RVB phase and the spin-reversal abnormal mode carrying both RVB and PB phases [4–6]. The momentum-dependent

geometric phase gradient causes the real-space photonics spin Hall shift, which can be calculated as (considering parallel polarization)

$$\delta_{\sigma}^y = \nabla_{k_{ry}} \Phi_{G,p}(\sigma) = -\nabla_{k_{ry}} \Phi_{Tot,p}(\sigma) = -\sigma \frac{\cot \theta}{k_0} \left(1 + \frac{r_s}{r_p} \right). \quad (\text{A3})$$

One can see from (A3) that it generates spin displacements with an equal magnitude but in opposite directions, which is the physical origin of the symmetric spin splitting. Note that Eq. (A3) is a rough calculation and is used for the qualitative analysis because it cannot represent the exact beam shifts where the incident angular spectrum should be considered. Considering the simplest beam, the Gaussian beam as the incident beam, the spin shifts can be exactly calculated from

Eq. (8) in the main text, as follows:

$$\delta_{\sigma}^y = -\sigma \frac{k_0 w_0^2 r_p \left(1 + \frac{r_s}{r_p} \right) \cot \theta}{k_0^2 w_0^2 r_p^2 + (r_p + r_s)^2 \cot^2 \theta}. \quad (\text{A4})$$

It is clearly seen that, when $k_0^2 w_0^2 \gg \cot \theta$, Eq. (A4) degenerates into Eq. (A3). Note that using the result of Eq. (A3) to analyze the PSHE is valid only for some general incident beams without any momentum-dependent phase. However, assuming the incident angular spectrum carrying the momentum-dependent phase $\Phi_{int,p}$, such as the LGB, one of the vortex beams, its total phase after reflection involves the initial phase and the geometric phase. The symmetric spin splitting in the reflected beam obviously no longer occurs due to the initial phase ($\Phi_{int,p} \neq 0$) and instead leads to an asymmetric photonic spin Hall shift result.

-
- [1] M. Onoda, S. Murakami, and N. Nagaosa, Hall Effect of Light, *Phys. Rev. Lett.* **93**, 083901 (2004).
- [2] K. Y. Bliokh and Y. P. Bliokh, Conservation of Angular Momentum, Transverse Shift, and Spin Hall Effect in Reflection and Refraction of an Electromagnetic Wave Packet, *Phys. Rev. Lett.* **96**, 073903 (2006).
- [3] K. Y. Bliokh, F. J. Rodriguez-Fortuno, F. Nori, and A. V. Zayats, Spin-orbit interactions of light, *Nat. Photon.* **9**, 796 (2015).
- [4] K. Y. Bliokh, Y. Gorodetski, V. Kleiner, and E. Hasman, Coriolis Effect in Optics: Unified Geometric Phase and Spin-Hall Effect, *Phys. Rev. Lett.* **101**, 030404 (2008).
- [5] K. Y. Bliokh, A. Niv, V. Kleiner, and E. Hasman, Geometrodynamics of spinning light, *Nat. Photon.* **2**, 748 (2008).
- [6] X. Ling, F. Guan, X. Cai, S. Ma, H.-X. Xu, Q. He, S. Xiao, and L. Zhou, Topology-induced phase transitions in spin-orbit photonics, *Laser Photon. Rev.* **15**, 2000492 (2021).
- [7] L. J. Kong, X. L. Wang, S. M. Li, Y. N. Li, J. Chen, B. Gu, and H. T. Wang, Spin Hall effect of reflected light from an air-glass interface around the Brewster's angle, *Appl. Phys. Lett.* **100**, 071109 (2012).
- [8] X. Zhou, X. Ling, H. Luo, and S. Wen, Identifying graphene layers via spin Hall effect of light, *Appl. Phys. Lett.* **101**, 251602 (2012).
- [9] S. Z. Chen, X. H. Ling, W. X. Shu, H. L. Luo, and S. C. Wen, Precision Measurement of the Optical Conductivity of Atomically Thin Crystals via the Photonic Spin Hall Effect, *Phys. Rev. Appl.* **13**, 014057 (2020).
- [10] M. Jiang, H. Lin, L. Zhuo, W. Zhu, H. Guan, J. Yu, H. Lu, J. Tan, and Z. Chen, Chirality induced asymmetric spin splitting of light beams reflected from an air-chiral interface, *Opt. Express* **26**, 6593 (2018).
- [11] M. Jiang, W. Zhu, H. Guan, J. Yu, H. Lu, J. Tan, J. Zhang, and Z. Chen, Giant spin splitting induced by orbital angular momentum in an epsilon-near-zero metamaterial slab, *Opt. Lett.* **42**, 3259 (2017).
- [12] S. Liu, S. Qi, Y. Li, B. Wei, P. Li, and J. Zhao, Controllable oscillated spin Hall effect of Bessel beam realized by liquid crystal Pancharatnam-Berry phase elements, *Light: Sci. Appl.* **11**, 219 (2022).
- [13] W. Zhu, L. Zhuo, M. Jiang, H. Guan, J. Yu, H. Lu, Y. Luo, J. Zhang, and Z. Chen, Controllable symmetric and asymmetric spin splitting of Laguerre-Gaussian beams assisted by surface plasmon resonance, *Opt. Lett.* **42**, 4869 (2017).
- [14] S. Liu, P. Li, Y. Zhang, X. Gan, M. Wang, and J. Zhao, Longitudinal spin separation of light and its performance in three-dimensionally controllable spin-dependent focal shift, *Sci. Rep.* **6**, 20774 (2016).
- [15] F. Wu, T. Liu, Y. Long, S. Xiao, and G. Chen, Giant photonic spin Hall effect empowered by polarization-dependent quasi-bound states in the continuum in compound grating waveguide structures, *Phys. Rev. B* **107**, 165428 (2023).
- [16] M. Shah, Probing topological quantum phase transitions via photonic spin Hall effects in spin-orbit coupled 2D quantum materials, *J. Phys. D: Appl. Phys.* **55**, 105105 (2021).
- [17] W. Xu, Q. Yang, G. Ye, W. Wu, W. Zhang, H. Luo, and S. Wen, Giant photonic spin Hall effect near the Dirac points, *Phys. Rev. A* **101**, 023826 (2020).
- [18] Y. Lin, X. Liu, H. Chen, X. Guo, J. Pan, J. Yu, H. Zheng, H. Guan, H. Lu, Y. Zhong, Y. Chen, Y. Luo, W. Zhu, and Z. Chen, Tunable asymmetric spin splitting by black phosphorus sandwiched epsilon-near-zero-metamaterial in the terahertz region, *Opt. Express* **27**, 15868 (2019).
- [19] Z. Chen, H. Zhang, X. Zhang, H. Li, J. Yang, W. Zhang, L. Xi, and X. Tang, Symmetric spin splitting of elliptically polarized vortex beams reflected at air-gold interface via pseudo-Brewster angle, *Opt. Express* **28**, 29529 (2020).
- [20] Z. Chen, H. Zhang, X. Zhang, H. Li, W. Zhang, and L. Xi, Cross-coupling effect induced beam shifts for polarized vortex beam at two-dimensional anisotropic monolayer graphene surface, *Opt. Express* **28**, 8308 (2020).
- [21] C. Liang, D. Liu, R. Liu, D. Deng, and G. Wang, Chirality-modulated photonic spin Hall effect in PT-symmetry, *Nanophotonics* **11**, 3475 (2022).
- [22] W. Luo, S. Xiao, Q. He, S. Sun, and L. Zhou, Photonic spin hall effect with nearly 100% efficiency, *Adv. Opt. Mater.* **3**, 1102 (2015).
- [23] T. F. Zhu, Y. J. Lou, Y. H. Zhou, J. H. Zhang, J. Y. Huang, Y. Li, H. L. Luo, S. C. Wen, S. Y. Zhu, Q. H. Gong, M. Qiu, and Z. C. Ruan, Generalized Spatial Differentiation from the Spin Hall Effect of Light and Its Application in Image Processing of Edge Detection, *Phys. Rev. Appl.* **11**, 034043 (2019).

- [24] J. Liu, Q. Yang, S. Chen, Z. Xiao, S. Wen, and H. Luo, Intrinsic Optical Spatial Differentiation Enabled Quantum Dark-Field Microscopy, *Phys. Rev. Lett.* **128**, 193601 (2022).
- [25] W. Shu, C. Lin, J. Wu, S. Chen, X. Ling, X. Zhou, H. Luo, and S. Wen, Three-dimensional spin Hall effect of light in tight focusing, *Phys. Rev. A* **101**, 023819 (2020).
- [26] S. S. Stafeev, A. G. Nalimov, A. A. Kovalev, V. D. Zaitsev, and V. V. Kotlyar, Circular polarization near the tight focus of linearly polarized light, *Photonics* **9**, 196 (2022).
- [27] Y. Shen, X. Wang, Z. Xie, C. Min, X. Fu, Q. Liu, M. Gong, and X. Yuan, Optical vortices 30 years on: OAM manipulation from topological charge to multiple singularities, *Light: Sci. Appl.* **8**, 90 (2019).
- [28] C. He, Y. Shen, and A. Forbes, Towards higher-dimensional structured light, *Light: Sci. Appl.* **11**, 205 (2022).
- [29] J. Ng, Z. Lin, and C. T. Chan, Theory of Optical Trapping by an Optical Vortex Beam, *Phys. Rev. Lett.* **104**, 103601 (2010).
- [30] Y. J. Yang, Y. X. Ren, M. Z. Chen, Y. Arita, and C. Rosales-Guzmán, Optical trapping with structured light: A review, *Adv. Photon.* **3**, 034001 (2021).
- [31] L. Allen, M. W. Beijersbergen, R. J. Spreeuw, and J. P. Woerdman, Orbital angular momentum of light and the transformation of Laguerre-Gaussian laser modes, *Phys. Rev. A* **45**, 8185 (1992).
- [32] M. Chen and F. S. Roux, Accelerating the annihilation of an optical vortex dipole in a Gaussian beam, *J. Opt. Soc. Am. A* **25**, 1279 (2008).
- [33] G. Indebetouw, Optical vortices and their propagation, *J. Mod. Opt.* **40**, 73 (1993).
- [34] F. S. Roux, Canonical vortex dipole dynamics, *J. Opt. Soc. Am. B* **21**, 655 (2004).
- [35] D. Rozas, C. T. Law, and G. A. Swartzlander, Propagation dynamics of optical vortices, *J. Opt. Soc. Am. B* **14**, 3054 (1997).
- [36] D. Rozas, Z. S. Sacks, and G. A. Swartzlander, Experimental Observation of Fluidlike Motion of Optical Vortices, *Phys. Rev. Lett.* **79**, 3399 (1997).
- [37] X. Zhou and X. Ling, Unveiling the photonic spin Hall effect with asymmetric spin-dependent splitting, *Opt. Express* **24**, 3025 (2016).
- [38] X. Zhou, L. Xie, X. Ling, S. Cheng, Z. Zhang, H. Luo, and H. Sun, Large in-plane asymmetric spin angular shifts of a light beam near the critical angle, *Opt. Lett.* **44**, 207 (2019).
- [39] X. Zhou, Y. Ding, J. Tu, J. Zhang, and D. Deng, Off-axis vortex-induced asymmetric spin-dependent splitting, *Ann. Phys. (Berlin)* **534**, 2200236 (2022).
- [40] W. Zhu, M. Jiang, H. Guan, J. Yu, H. Lu, J. Zhang, and Z. Chen, Tunable spin splitting of Laguerre-Gaussian beams in graphene metamaterials, *Photon. Res.* **5**, 684 (2017).
- [41] S. Qi and H. Da, Controllable photonic spin Hall effect of bilayer graphene, *Nanotechnology* **33**, 315201 (2022).
- [42] K. Y. Bliokh and A. Aiello, Goos-Hänchen and Imbert-Fedorov beam shifts: An overview, *J. Opt.* **15**, 014001 (2013).